tvst

Article

Potential-Driven Electrochemical Clearing of Ex Vivo Alkaline Corneal Injuries

Katelyn K. Dilley[1,2], Pamela A. Borden[1,2], Yueqiao Qu[1,2], Andrew E. Heidari[1,2], Karthik R. Prasad[1,3], Yan Li[1,2], Chung Ho Sun[1], Zhongping Chen[1,2], Sehwan Kim[4], Michael G. Hill[5], and Brian J. F. Wong[1,2,6]

[1] Beckman Laser Institute & Medical Clinic, University of California–Irvine, Irvine, CA, USA
[2] Department of Biomedical Engineering, University of California–Irvine, Irvine, CA, USA
[3] School of Medicine, University of California–Irvine, Irvine, CA, USA
[4] Beckman Laser Institute-Korea, Department of Biomedical Engineering, Dankook University, Cheonan-si, Chungnam, Republic of Korea
[5] Department of Chemistry, Occidental College, Los Angeles, CA, USA
[6] Department of Otolaryngology–Head and Neck Surgery, University of California–Irvine, School of Medicine, Orange, CA, USA

Correspondence: Brian J.F. Wong, University of California, Irvine, 1002 Health Sciences Rd, Irvine, CA 92612, USA. e-mail: bjwong@uci.edu

Received: July 15, 2021
Accepted: December 17, 2021
Published: January 21, 2022

Keywords: alkaline injury; corneal clearing; potential-driven electrochemical treatment; optical coherence tomography; second harmonic generation

Citation: Dilley KK, Borden PA, Qu Y, Heidari AE, Prasad KR, Li Y, Sun CH, Chen Z, Kim S, Hill MG, Wong BJF. Potential-driven electrochemical clearing of ex vivo alkaline corneal injuries. Transl Vis Sci Technol. 2022;11(1):32, https://doi.org/10.1167/tvst.11.1.32

Purpose: Corneal chemical injuries (CCI) obscure vision by opacifying the cornea; however, current treatments may not fully restore clarity. Here, we investigated potential-driven electrochemical treatment (P-ECT) to restore clarity after alkaline-based CCI in ex vivo rabbit corneas and examined collagen fiber orientation changes using second harmonic generation (SHG).

Methods: NaOH was applied to the corneas of intact New Zealand white rabbit globes. P-ECT was performed on the opacified cornea while optical coherence tomography (OCT) imaging (~35 frames per second) was simultaneously performed. SHG imaging evaluated collagen fiber structure before NaOH application and after P-ECT. Irrigation with water served as a control.

Results: P-ECT restored local optical clarity after NaOH exposure. OCT imaging shows both progression of NaOH injury and the restoration of clarity in real time. Analysis of SHG z-stack images show that collagen fibril orientation is similar between control, NaOH-damaged, and post-P-ECT corneas. NaOH-injured corneas flushed with water (15 minutes) show no restoration of clarity.

Conclusions: P-ECT may be a means to correct alkaline CCI. Collagen fibril orientation does not change after NaOH exposure or P-ECT, suggesting that no irreversible matrix level fiber changes occur. Further studies are required to determine the mechanism for corneal clearing and to ascertain the optimal electrical dosimetry parameters and electrode designs.

Translational Relevance: Our findings suggest that P-ECT is a potentially effective, low-cost treatment for alkaline CCI.

Introduction

Corneal chemical injuries (CCI) make up between 11% to 22% of all ocular injuries.[1] Currently, CCI are treated by flushing the eye with fluids to remove the chemical irritant and restore physiological pH. For mild cases, simply flushing the eye continuously with water for 20 minutes immediately after injury can greatly improve outcomes.[2] In moderate cases of corneal chemical injury, physicians often use topical prednisolone acetate and broad-spectrum antibiotics to treat inflammation and potential bacterial infection.[3] Unfortunately, 4.1% of patients with severe chemical burns must undergo corneal transplantation to remove necrotic tissue and to restore vision.[4] Many high-grade corneal transplant patients, on recovery, suffer from glaucoma, hypotony, and cataracts when their cornea heals, which results in vision compromise.[5] Hence, there exists a need for additional methods to

potentially reduce the severity of CCI early on and reduce the progression of injury to where transplantation is the only option.

Direct corneal surface electrolysis has been used to correct corneal and subepithelial opacities that formed after lamellar keratoplasty and penetrating keratoplasty, respectively.[6,7] Opacities were cleared by placing an anode and NaCl-soaked gauze on the patient's forehead, while a flat cathode was placed on the corneal deposits; although the cornea was continuously irrigated with saline solution, an electrolyzing voltage was applied, producing hydrogen gas and hydroxide at the cathode. This allowed for the controlled breakdown of the corneal deposits, which resulted in a cleared cornea. Here we expand the use of tissue electrochemistry using potential-driven electrochemical corneal clearing (P-ECC) and aim to treat alkaline injury via the selective and controlled production of acid at the corneal surface to reverse base-induced CCI.

The concept of exploiting reduction-oxidation chemical reactions in situ to alter tissue biophysical properties was first presented in 2003, and extensive work was focused on using this technology, termed *electromechanical reshaping*, in the alteration of cartilage structure.[8] Other tissues may undergo similar transformations using either contact or needle electrodes in which a potential may be applied, leading to water hydrolysis, local acid and base production, and subsequent changes in tissue macromolecular structure. In cartilage this leads to shape change; in tendon this leads to shape change, as well as changes in Young's modulus; in skin matrix collagen structure is altered; and in fat adipocyte cell membranes are lysed, and triglycerides are saponified.[9–29]

The need for altering the shape in various structures of the human body is limited to aesthetic features of the face and in tendon, ligament, and fat. Corneal modification could also be potentially important; however, there is an additional challenge that optical clarity must be maintained. Here, we examine the change in corneal thickness measured through optical coherence tomography (OCT) after the most common type of CCI is emulated, base injury, and electrochemical correction through P-ECC in rabbit cornea and examine collagen fibril orientation using second harmonic generation (SHG).[30–32]

Methods

Extraction and use of Specimen

Intact eye globes were extracted from the crania of New Zealand white rabbits euthanized under other UC Irvine IACUC protocols. Globes were extracted within three hours of euthanization and placed in sterile saline solution at room temperature; experiments began within two hours.

SHG and Collagen Fibril Analysis

SHG was performed on native tissue before and after P-ECC treatment. These images served as controls for corneal structure and for identifying any existing superficial corneal injuries caused by scratches either before euthanasia or from the instrumentation, extraction, or transport. The globe was placed cornea facing downward into a transparent cell culture dish containing saline solution–soaked pieces of sponge for stabilization. The entire assembly was positioned on the viewing platform of an inverted Zeiss LSM 510 Meta Confocal Microscope (Zeiss, Oberkochen, Germany),and images were recorded using an excitation wavelength of 920 nm. SHG z-stacks (900 μm × 900 μm), taken of an average thickness of 150 μm with 10 μm/step, were processed through FIJI open source imaging software using the OrientationJ plugin.[33] This plugin characterizes the orientation and isotropy properties of the collagen in the image by evaluating the gradient structure tensor of the local neighborhood of the selected image, and orientation angles may range from −90° to +90°. MATLAB was then used to center the data through an artificially generated 0°. The data were normalized against the lowest observed frequencies; the number of occurrences were converted into normalized decimal numbers ranging from 0 to 1, allowing direct comparison between all datasets. To accommodate for the potential changes in the cornea placement during the two imaging sessions, additional analysis isolating a region of interest (ROI) by stacking the concentric tile images to identify a reference area was performed to directly compare the z-stacks of the control and treated corneal centers.

OCT and Potential-driven Electrochemical Therapy (P-ECT)

OCT was used to image the tissue before treatment, as well as during chemical injury and subsequent potential-driven electrochemical therapy.[34,35] A spectral domain OCT imaging device was used to capture three-dimensional structures with a lateral resolution of 11.78 μm and axial resolution of 3.5 μm; it acquired single-plane dynamic B-Scan images each comprised of 1000 a-lines distributed across a 6 mm cross-section.[36] The region surrounding the treatment

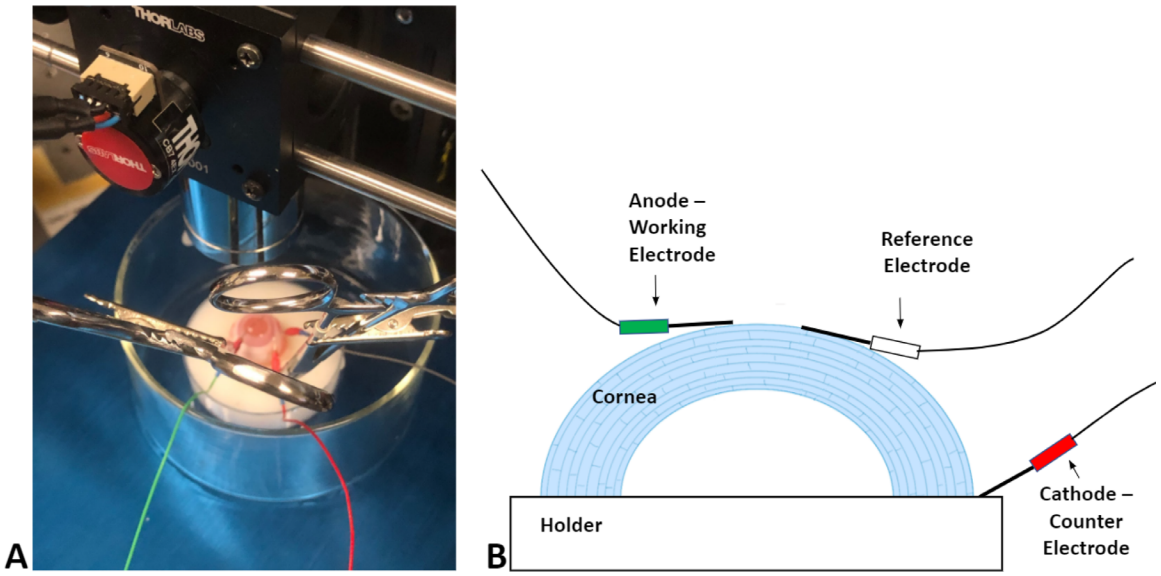

Figure 1. Experimental setup for ECT while OCT is running continuously during treatment. (**A**) Digital picture and (**B**) drawn diagram of the layout.

electrode was imaged to sufficiently visualize the effect of the acid on the cornea. A total of approximately 45,000 images were acquired spanning the entirety of the experiment from baseline (native state) to base injury and finally to the electrochemical clearing of the cornea.

Saline solution–soaked blotter paper was placed along the concave portion of a customized silicone jig to help preserve moisture and aid in positioning. The globe was then placed cornea side up in the jig and was then transferred into a clear container placed on a Y-axis adjustable stage to allow for beam positioning (Fig. 1A). OCT was performed continuously throughout each experiment to visualize stromal damage and corneal clearing.

Three platinum electrodes were used to perform P-ECC. The working electrode was laid flat, directly across the center of the cornea. The counter electrode was inserted between the eye and the hollow of the concave portion of the jig. The reference electrode was placed in close proximity to the working electrode in contact with the cornea (Fig. 1B). The P-ECT system parameters were set to run the specified voltage for each experiment; for control experiments, no voltage was applied to the corneal surface. The sample had 1.5 mL of 10 M NaOH pipetted onto the surface to simulate deep stromal alkaline damage. Exposure to the base lasted for approximately 60 seconds. The damaged cornea was flushed with room-temperature tap water and continued to be rinsed using a pipette for 10 minutes to simulate commonly directed treatment. A set of samples was set aside after NaOH exposure and flushing as the negative control group for comparison.

Using the P-ECT system (Model 650, CH instruments, Inc.), bulk electrolysis was performed at 1.5 to 2V for approximately 10 to 15 minutes or until the cleared region reached the edges of the monitor in the OCT image. These samples (NaOH-damaged + ECT-treated) were used as the experimental group against the control and negative control samples. SHG was performed to determine the structure of collagen after damage, ECT, or both. The treated eyes were then fixed in 10% formalin, and data analysis was performed on the OCT and SHG images. Corneal thickness analysis on the OCT images was completed through FIJI, and collagen alignment was analyzed using the OrientationJ plug-in and MATLAB.

Measuring Corneal pH

A separate set of eyes was used for pH trials, which were done to visualize the pH impact of P-ECC. This set of eyes includes an undamaged eye, NaOH damaged eye, NaOH damaged and flushed eye, and NaOH damaged and P-ECT treated eye. One drop of Hydrion pH indicator solution was administered to each eye. The color on the cornea was matched to the indicator chart to determine the pH.

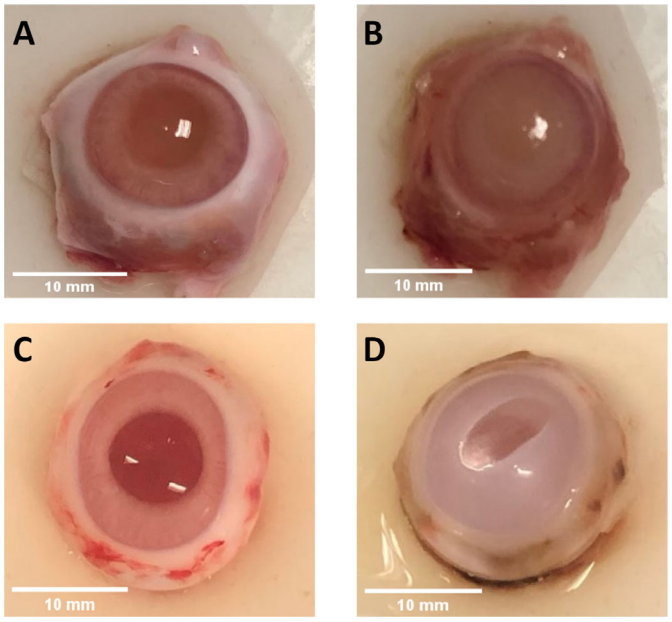

Figure 2. Optical images of the rabbit cornea (**A**) before and (**B**) after NaOH damage. Rabbit cornea opacity (**C**) before and (**D**) after NaOH damage and P-ECT treatment.

Results

Digital Photography of the Cornea and pH Measurements

Digital images of the native cornea show optical clarity with no obvious defects or deformities as expected (Figs. 2A, 2C). After application of the NaOH solution, opacification readily occurs and is consistent with a Hughes classification grade III/IV injury (Fig. 2B). Such an injury would generally require surgical treatment (e.g., transplant).[3] After P-ECT, optical clarity is restored in the region immediately adjacent to the anode electrode (Fig. 2D).

Figure 3A depicts healthy native cornea, and Figure 3B indicates that native cornea has an approximately neutral pH (yellow/green). NaOH damage, even after flushing with water, resulted in a basic pH (dark blue) (Figs. 3C, 3D, respectively). P-ECT treatment restored approximately neutral pH to the treated region (Fig. 3F), when compared to the middle of the cornea in Figure 3B.

OCT Imaging, Corneal Thickness, and the Effect of P-ECT

OCT images of native cornea reveal a relatively thin and gently curved structure on cross-section (Fig. 4A). The working electrode is indicated by arrows in Figure 1B at the central corneal surface. The addition of NaOH creates immediate corneal injury, and OCT reveals thickening and increased scattering (white signal intensity) seen in Figure 4B. When P-ECT is then performed in the damage zone, OCT shows reversal of localized swelling and the return

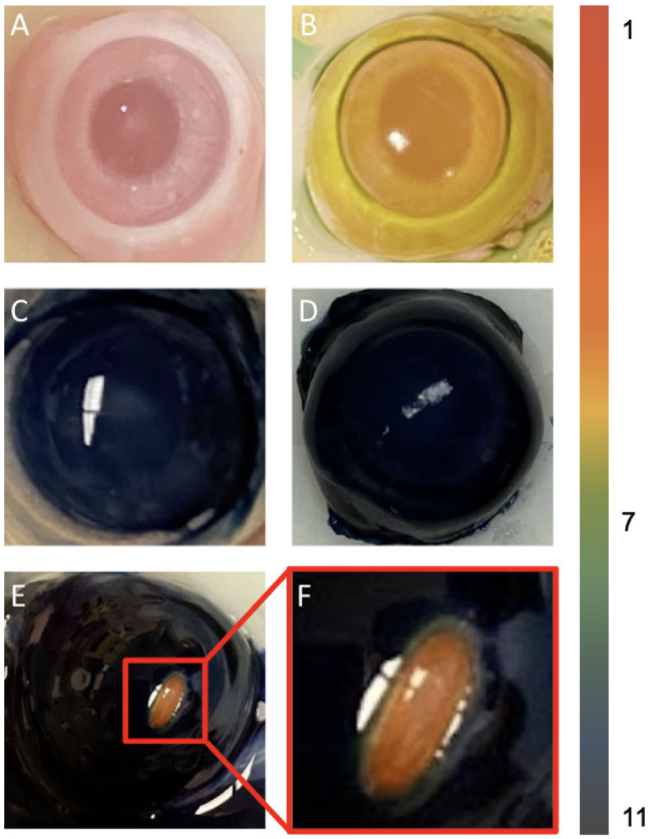

Figure 3. Images of pH trials on rabbit cornea: (**A**) Undyed native cornea, (**B**) dyed native cornea, (**C**) dyed NaOH-damaged cornea, (**D**) dyed NaOH-damaged and water-flushed cornea, (**E**) dyed NaOH-damaged and P-ECT–treated cornea, and (**F**) close up of P-ECT–treated region. A color scale indicating the corresponding pH is on the right.

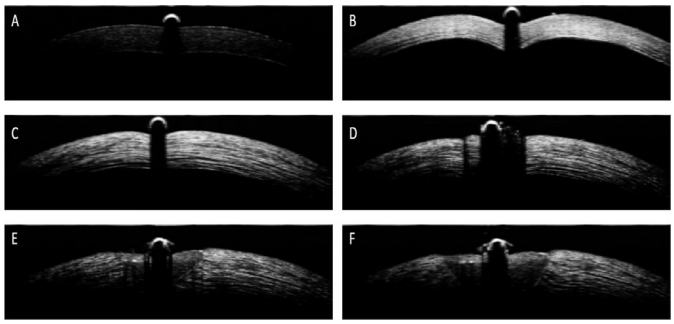

Figure 4. Optical images obtained via OCT showing the eye (**A**) undamaged (control), (**B**) immediately after NaOH damage, (**C**) after NaOH damage and flushing, (**D**) during the beginning of P-ECT clearing, (**E**) in the middle of P-ECT clearing, and (**F**) at the end of P-ECT clearing.

of optical clarity (Figs. 4C–F). The overall series of images demonstrate the clearing initially occurs where the working electrode is placed; it continues along the cornea via a ripple effect (see Supplementary Video S1). During clearing, gas bubbles (hydrogen) can be seen as soon as P-ECT begins at the working electrode. Thickness calculated from the captured OCT image (Fig. 4C) was 354.7 µm, which is an increase of 130.7 µm from the baseline of 224 µm seen in Figure 4A. After P-ECT, a corneal thickness of 319 µm measured in Figure 4F, a 35.7 µm reduction from Figure 4C.

SHG Imaging, Collagen Signal Intensity, and Fibril Alignment

SHG images of a healthy cornea exhibit a bright blue signal, showing that there is an abundance of collagen fibers (Figs. 5A, 5E). Small regions of low signal intensity were observed on some images and likely were due to injury produced from maneuvers associated with removing the eye from the rabbit and other preparatory steps in vivisection. An alkaline injury eliminated the SHG signal across the surface because significantly less collagen signal was detected. Absence of SHG signal (blue) indicates that structure of the collagen fibers has been disrupted. P-ECT treatment after NaOH damage resulted in the return of SHG signal in the region where bulk electrolysis was performed. The edges of the cornea, where diffusion of agents may have been inadequate, show little or no return of the collagen SHG signal.

SHG z-stacks (900 µm × 900 µm) imaged at the center of the cornea were acquired for the control, NaOH-damaged, and NaOH-damaged + P-ECT–treated eyes. These were then analyzed to determine the collagen fibril orientations throughout all imaged layers. The resulting histograms seen in Figure 5 demonstrate that the collagen fiber orientation retains a Gaussian distribution for all conditions at a depth of 150 µm from the cornea surface. For example, the introduction of NaOH minimally affected the cornea by increasing the preferred mean collagen orientation angle by approximately 2.13°, as well as increasing the standard deviation for the directionality by about 1.77° from the control sample. After the control eye received NaOH damage + P-ECT treatment, the standard deviation of directionality was nearly the same whereas the preferred mean collagen orientation angle decreased by 3.93°. Furthermore, depth-resolved orientation analysis shows that although collagen directionality decreased overall throughout the thickness of the cornea for the NaOH-damaged + P-ECT–treated samples, a major shift in fibril orientation was not seen (Fig. 6). These results indicate that the cornea's collagen organization and alignment are minimally affected by the introduction of NaOH and acid generated from the ECT treatment. Therefore collagen organization is likely not directly responsible for the optical change accompanying the clearing process. A summary of these degree comparisons can be seen in the Table.

Additional image analysis was performed to confirm the modest changes in collagen orientation between the control and treated samples observed in z-stack analysis. Tiled SHG images (Fig. 7) were acquired of the entire corneal surface before and after the experimental interventions. These tiled images were overlaid and positioned to ensure the selected region of interest z-stacks acquired at the center were in registration. Through the FIJI plugin OrientationJ, a function called *Measure* was used for processing to determine the ROI's coherency coefficient (Table) for the different experimental protocols. OrientationJ indicates that an ROI is highly organized in a preferred orientation if the calculated coefficient is close to 1.[37] The negative control sample of NaOH experienced no change in its tissue's coherency against the control cornea and showed no preferred orientation. The NaOH-damaged + P-ECT sample did have a decreased coherency coefficient against the control cornea by 0.1, but this value does not show a significant change in preferred orientation of the collagen fibers.

Discussion

This study suggests that P-ECT may clear the cornea after acute alkaline CCI, and the process does not alter cornea structure at the level of the constituent collagen molecules. Signal intensity for collagen in the SHG images decreased after exposure to NaOH and then returned after the P-ECT clearing process. Minute changes of collagen fibril's orientation was observed, but the effect is very small. Minimal difference between fibril orientations in control (native), negative control (NaOH-damaged only), and experimental sample (NaOH-damaged + P-ECT) fibril orientations suggests that the collagen organization in the matrix is not the critical mechanism for corneal opacity (or clearing) in this injury model.

A potential mechanism for corneal opacity is linked to the correction of the pH gradient imbalance created by an alkaline injury, because alkaline solutions are lipophilic and easily penetrate the cornea.[38] Traditional treatment of alkaline injuries is irrigation of the eye with water or a saline solution to normalize the pH

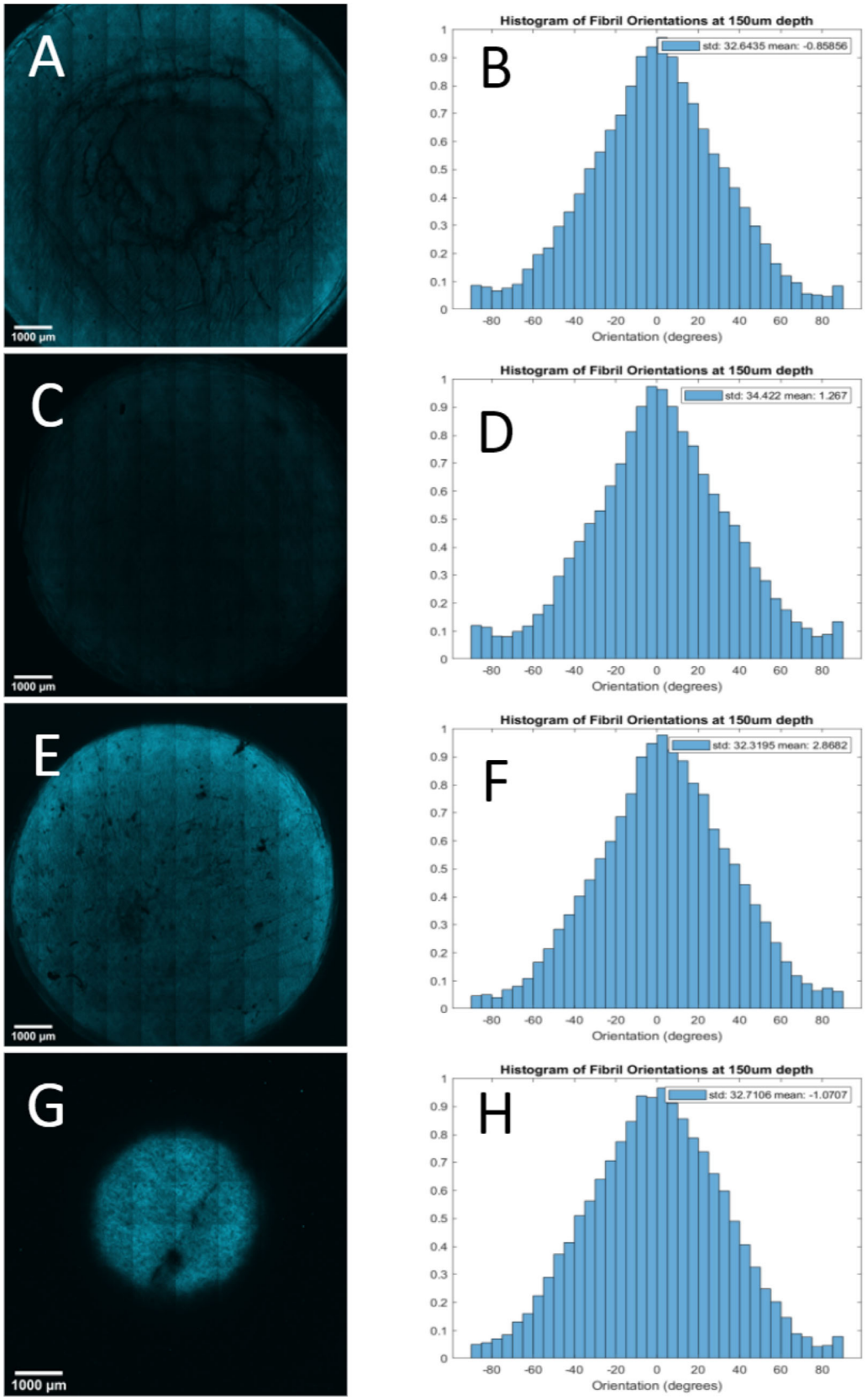

Figure 5. Tile SHG images to analyze the collagen alignment comparison between (**A**) native cornea and (**C**) NaOH-damaged and (**E**) native cornea against (**G**) NaOH-damaged + P-ECT–treated samples. Using FIJI on the z-stacks taken at the center of each cornea, histograms were generated to show the preferred orientation angles calculated at each step depth with representation at 150 µm deep (**B**, **D**, **F**, and **H**).

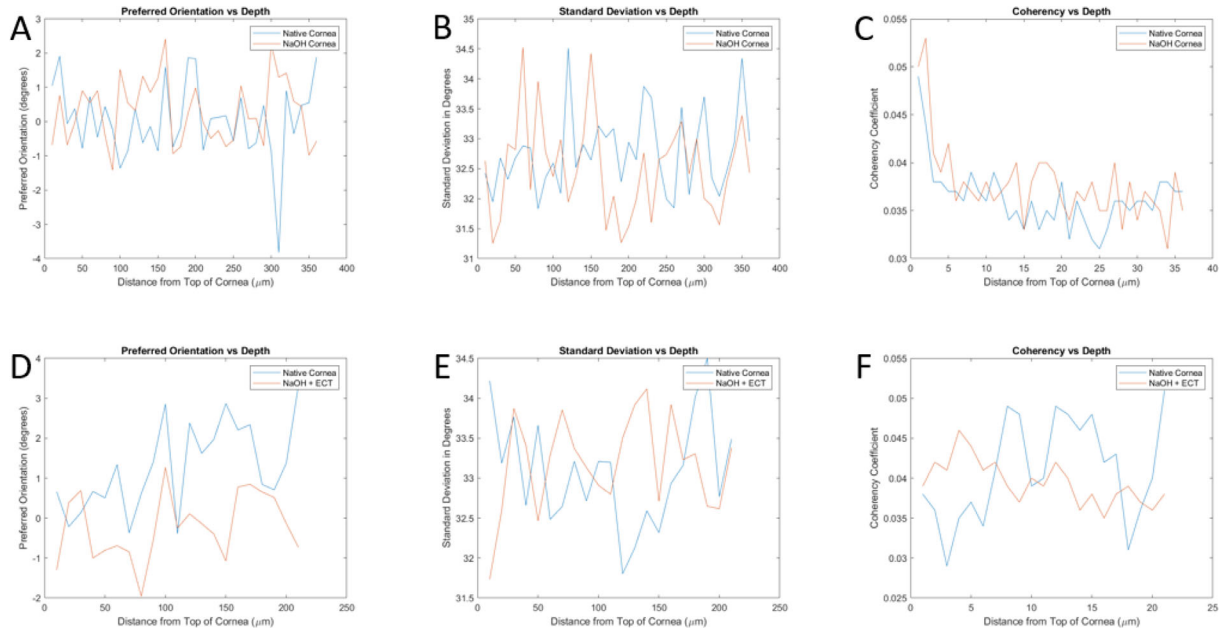

Figure 6. Collagen preferred (**A**) orientation, (**B**) standard deviation, and (**C**) coherency analyzed with respect to depth in NaOH-damaged corneas (*red line*) compared with its control (*blue line*). Data analysis was also performed on NaOH-damaged + P-ECT–treated tissues (**D**, **E**, **F**). Results show there is no significant pattern determined between the control, NaOH-damaged, and NaOH-damaged + P-ECT–treated corneas because orientation appears to be randomized throughout the imaged corneal thickness.

Table. Comparison of Collagen Orientation (Means, Standard Deviation, and Coherency)

Protocol	Collagen Orientation Mean	Collagen Orientation Standard Deviation	Coherency
Control*	−0.85856°	32.6435°	0.033
NaOH*	1.267°	34.422°	0.033
Control†	2.8682°	32.3195°	0.048
NaOH + P-ECT†	−1.0707°	32.7106°	0.038

Comparison of collagen orientation in SHG images taken at 150 µm depth of control and experimental corneas analyzed through ImageJ for collagen fibril orientation mean and standard deviation.

*P value = 0.29 (one-way ANOVA).

†P value = 1.32e-05 (one-way ANOVA).

and remove particulates. However, irrigation of the eye may not normalize pH changes within the stroma, and in fact overirrigation may result in corneal edema. Immediate swelling of the cornea during alkaline injury is evident during the analysis of the collected OCT data as an increase in thickness of approximately 130 µm. Figure 8 is a schematic representation of the changes that may occur in the collagen, with swelling but overall preservation of structural and orientation at the tertiary level. The change in thickness may contribute to the opacity of the cornea as the tissue swells, increasing scatter as light passes through the swollen tissue.

To potentially address corneal opacity resulting from relatively acute alkaline injury, P-ECT can be used to normalize pH as the anode is used as the working electrode, resulting in local acid production from the electrolysis of water. As the water is split, the swelling of the collagen fibrils decreases around the electrode, which is seen in OCT imaging from Figures 4C to 4E where the area adjacent to the anode contracts by 35.7 microns. The electrolysis of base and acid at the anode and cathode sites results in the production of water molecules which leads to a decrease in interstitial ionic strength and osmosis out of the stroma. This process is spatially selective and a

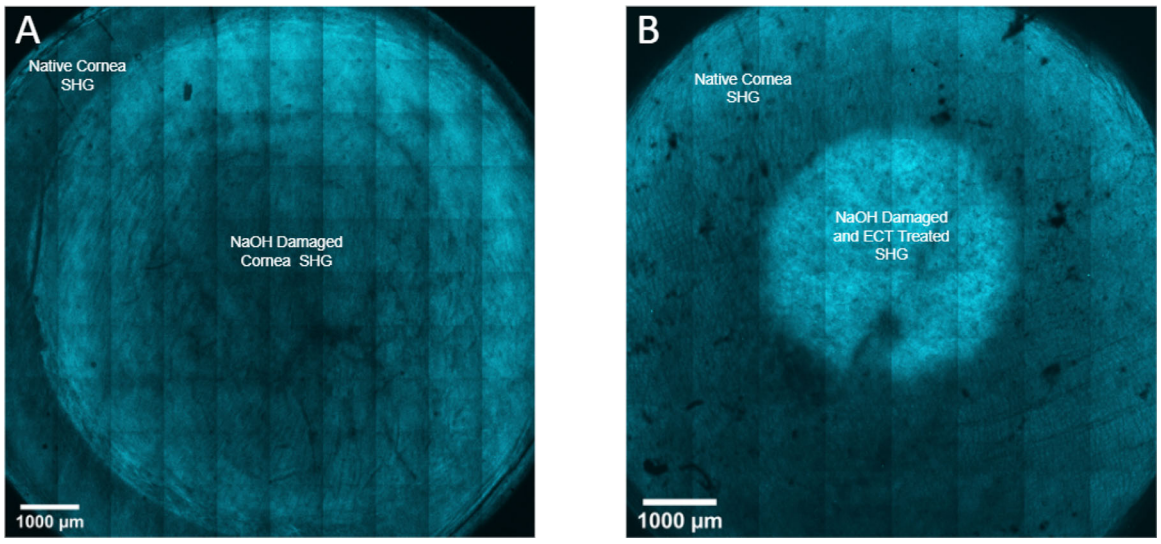

Figure 7. Overlay of SHG-imaged control corneas with (**A**) NaOH-damaged and (**B**) NaOH-damaged + P-ECT–treated corneas. Area of post-NaOH damaged cornea is significantly smaller than the control because of the rigidity of the tissue after exposure, resulting in less surface area of the cornea coming into contact with the microscope slide.

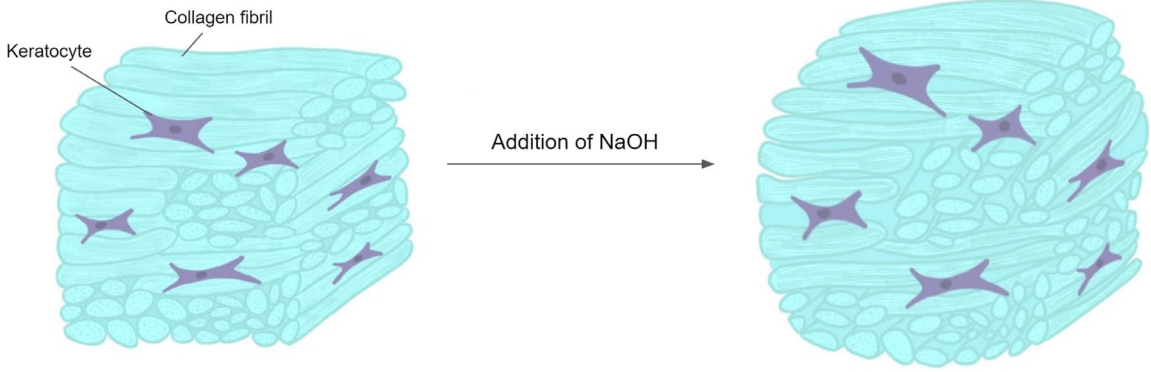

Figure 8. Schematic illustration representing the swelling of the collagen fibers after alkaline injury of the cornea.

function of the electrode field geometry and diffusion over a relatively small spatial scale. The field geometry is in turn dictated by electrode design and the applied potential. Prudent electrode design may yield a clinically relevant device that could easily be used by physicians and healthcare extenders such as paramedics and nurse practitioners at the point of care in industrial accidents. P-ECT has been previously used to reshape cartilage and modify the microstructure of skin and fat.[39]

This potential process is rapid and minimally invasive because voltage is applied from 5 to 20 minutes using electrodes placed on the tissue's surface to address the region of interest. P-ECT is a low-cost technology because electrodes are inexpensive and could be accomplished with a DC power source (watch battery) or with modest cost and complexity, an operation amplifier circuit (~$1.00).

A limitation of this pilot study is that analysis was performed using exclusively OCT and SHG imaging. These imaging techniques are structural, resolving anatomy at different spatial scales and rely on different means of endogenous contrast. SHG does have intrinsic limitations, mainly how data are registered. Additionally, imprecise registry of SHG z-stacks may potentially lead to an inaccurate comparison between control and experimental samples. The step depth during microscopy used in this protocol may be too large and miss the affected area, or sample alignment may change during its removal, treatment, and then replacement on the imaging stage. Registry is a challenge because data are three dimensional, and

with injury and correction, swelling occurs and is then reduced. Although nonlinear optical microscopy and OCT imaging of native tissue do not require fixation or dyes, these techniques do not provide information on cellular function or viability (beyond NADH/NADPH status), which would in general require fluorescence or antibody methods. Classic light microscopy needs to be performed as well. Fluorescent imaging will need to be used to map and quantify the viability of the cells after base injury and determine if the P-ECT process created additional injury or damage. We plan to pursue this in the future.

There are many parameters involved with P-ECT, and only limited information is garnered from studies focused on cartilage, fat, skin, and tendon because these are very different tissues from cornea. Although P-ECT can be used in each of the aforementioned tissues to alter stress-strain relationships, viability, or shape, the cornea is unique in that the preservation of optical clarity (or its restoration) remains the paramount objective. Electrical potential, application time, pulse sequence, electric field geometry, and electrode configuration all are independent variables here. Identifying electrical dosimetry parameters and electrode designs that lead to consistent clearing outcomes and predictable results will be the important steps before this technology can be evaluated in in vivo animal studies.

In conclusion, P-ECT to correct corneal opacity after alkaline CCI is an interesting biophysical process that may have clinical application in the future. After simulating alkaline injury, our SHG imaging suggests that opacities within the cornea result from excess tissue swelling without extensive collagen denaturation, at least at the tertiary level of the molecule. Through P-ECT, water is split at the electrode site, and acid is created to counter pH changes to reduce swelling and restore collagen's structure. Accordingly, corneal P-ECT may lead to low-cost, point-of-care devices that may have value in treating severe chemical injuries that may be encountered in industrial and military settings. This may allow for the reversal of corneal opacity from acute injury and better recovery from alkaline CCIs where irrigation has remained the treatment of choice for more than a millennia.

Acknowledgments

The authors thank Tanya Burney and Dave Mukai for providing the rabbit eye samples used in this study.

Supported by the UCI BEAL Applied Innovation Proof of Product (POP) Grant Award, Wayfinder UCI IP Based Startup Grant Award (Supported by the Nicholas Foundation), National Institutes of Health/National Institute of Biomedical Imaging and Bioengineering (NIH/NIBIB) (R01EB030024), National Institutes of Health/National Institute of Biomedical Imaging and Bioengineering (NIH/NIBIB) (P41EB015890), National Institutes of Health/National Institute of Biomedical Imaging and Bioengineering (NIH/NIBIB) (R01HL-125084), National Institutes of Health/National Institute of Biomedical Imaging and Bioengineering (NIH/NIBIB) (R01EB-030024), National Institutes of Health from the National Eye Institute (NIH/NEI) (1R15EY032273-01), Air Force Office of Scientific Research (FA9550-20-1-0052), the UCI School of Medicine's Dean's Summer Research Scholarship, the Leading Foreign Research Institute Recruitment Program through the National Research Foundation of Korea (NRF) funded by the Ministry of Science and ICT (MSIT) (NRF-2018K1A4A3A02060572), and the UCI Undergraduate Research Opportunities Program.

Disclosure: **K.K. Dilley**, None; **P.A. Borden**, None; **Y. Qu**, None; **A.E. Heidari**, None; **K.R. Prasad**, None; **Y. Li**, None; **C. Sun**, None; **Z. Chen**, OCT Medical Imaging Inc. (I, C, P, S); **S. Kim**, None; **M.G. Hill**, None; **B.J.F. Wong**, None

References

1. Clare G, Suleman H, Bunce C, Dua H. Amniotic membrane transplantation for acute ocular burns. *Cochrane Database Syst. Rev*. 2012;(9):CD009379.
2. Lubeck D, Greene JS. Corneal injuries. *Emerg Med Clin North Am*. 1988;6:73–94.
3. Hemmati HD, Colby KA. Treating acute chemical injuries of the cornea. *Am Acad Ophthalmol*. 2012:43–45.
4. Ghosh S, Kotagiri A, Pushpoth S, Tey A, Johnson Z, Figueiredo F. Chemical injuries of the eye—clinical study of 98 consecutive cases. *Invest Ophthalmol Vis Sci*. 2010;51:5382–5382.
5. Wagoner MD. Chemical injuries of the eye: current concepts in pathophysiology and therapy. *Surv Ophthalmol*. 1997;41:275–313.
6. Mashima Y. Corneal electrolysis for recurrence of corneal stromal dystrophy after keratoplasty. *Br J Ophthalmol*. 2002;86:273–275.
7. Mashima Y, Kawashima M, Yamada M. Electrolytic removal of recurrence of granular corneal dystrophy. *Eye*. 2003;17:975–981.

8. Ho K-HK, Valdes SH, Protsenko DE, Aguilar G, Wong BJ. Electromechanical reshaping of septal cartilage. *Laryngoscope*. 2010;113:1916–1921.
9. Protsenko DE, Ho K, Wong BJ. Stress relaxation in porcine septal cartilage during electromechanical reshaping: mechanical and electrical responses. *Ann Biomed Eng*. 2006;34:455–464.
10. Manuel CT, Foulad A, Protsenko DE, Sepehr A, Wong BJ. Needle electrode-based electromechanical reshaping of cartilage. *Ann Biomed Eng*. 2010;38:3389–3397.
11. Protsenko DE, Ho K, Wong BJ. Survival of chondrocytes in rabbit septal cartilage after electromechanical reshaping. *Ann Biomed Eng*. 2010;39:66–74.
12. Manuel CT, Foulad A, Protsenko DE, Hamamoto A, Wong BJ. Electromechanical reshaping of costal cartilage grafts: a new surgical treatment modality. *Laryngoscope*. 2011;121:1839–1842.
13. Wu EC, Protsenko DE, Khan AZ, Dubin S, Karimi K, Wong BJ. Needle-electrode-based electromechanical reshaping of rabbit septal cartilage: a systematic evaluation. *IEEE Trans Biomed Eng*. 2011;58:2378–2383.
14. Lim A, Protsenko DE, Wong BJ. Changes in the tangent modulus of rabbit septal and auricular cartilage following electromechanical reshaping. *J Biomech Eng*. 2011;133(9):094502.
15. Oliaei S, Manuel C, Karam B, et al. In vivo electromechanical reshaping of ear cartilage in a rabbit model. *JAMA Facial Plast Surg*. 2013;15:34–38.
16. Badran K, Manuel C, Waki C, Protsenko D, Wong BJ. Ex vivo electromechanical reshaping of costal cartilage in the New Zealand white rabbit model. *Laryngoscope*. 2013;123:1143–1148.
17. Yau AY, Manuel C, Hussain SF, Protsenko DE, Wong BJ. In vivo needle-based electromechanical reshaping of pinnae. *JAMA Facial Plast Surg*. 2014;16:245–252.
18. Hussain S, Manuel CT, Protsenko DE, Wong BJ. Electromechanical reshaping of ex vivo porcine trachea. *Laryngoscope*. 2015;125:1628–1632.
19. Badran KW, Manuel CT, Loy AC, et al. Long-term in vivo electromechanical reshaping for auricular reconstruction in the New Zealand white rabbit model. *Laryngoscope*. 2015;125:2058–2066.
20. Kuan EC, Hamamoto AA, Manuel CT, Protsenko DE, Wong BJ. In-depth analysis of pH-dependent mechanisms of electromechanical reshaping of rabbit nasal septal cartilage. *Laryngoscope*. 2014;124(10):E405–E410.
21. Hunter BM, Kallick J, Kissel J, et al. Controlled-potential electromechanical reshaping of cartilage. *Angew Chem Int Ed Engl*. 2016;55:5497–5500.
22. Manuel CT, Tjoa T, Nguyen T, Su E, Wong BJ. Optimal electromechanical reshaping of the auricular ear and long-term outcomes in an in vivo rabbit model. *JAMA Facial Plast Surg*. 2016;18:277–284.
23. Nguyen TD, Hu AC, Protsenko DE, Wong BJF. Effects of electromechanical reshaping on mechanical behavior of exvivo bovine tendon. *Clin Biomechan*. 2020;73:92–100.
24. Moy WJ, Su E, Chen JJ, et al. Association of electrochemical therapy with optical, mechanical, and acoustic impedance properties of porcine skin. *JAMA Facial Plast Surg*. 2017;19:502–509.
25. Hu AC, Hong EM, Toubat O, et al. Multiphoton microscopy of collagen structure in ex vivo human skin following electrochemical therapy. *Lasers Surg Med*. 2019;52:196–206.
26. Pham TT, Hong EM, Moy WJ, et al. The biophysical effects of localized electrochemical therapy on porcine skin. *J Dermatol Sci*. 2020;97:179–186.
27. Hutchison DM, Hakimi AA, Wijayaweera A, et al. Electrochemical treatment of ex vivo human abdominal skin and potential use in scar management: a pilot study. *Scars Burn Heal*. 2021;7:2059513120988532.
28. Hutchison DM, Hakimi AA, Hong EM, et al. Electrochemolipolysis of human adipose tissue. *Facial Plast Surg Aesthet Med*. 2020;22:86–92.
29. Pham TT, Stokolosa AM, Borden PA, et al. Electrochemical degradation and saponification of porcine adipose tissue. *Sci Rep*. 2020;10(1):20745.
30. Singh P, Tyagi M, Kumar Y, Gupta KK, Sharma PD. Ocular chemical injuries and their management. *Oman J Ophthalmol*. 2013;6(2):83.
31. Chen X, Nadiarynkh O, Plotnikov S, Campagnola PJ. Second harmonic generation microscopy for quantitative analysis of collagen fibrillar structure. *Nat Protoc*. 2012;7:654–669.
32. Park CY, Lee JK, Chuck RS. Second harmonic generation imaging analysis of collagen arrangement in human cornea. *Invest Ophthalmol Vis Sci*. 2015;56:5622–5629.
33. Rezakhaniha R, Agianniotis A, Schrauwen JT, et al. Experimental investigation of collagen waviness and orientation in the arterial adventitia using confocal laser scanning microscopy. *Biomechan Model Mechanobiol*. 2011;11(3-4):461–473.
34. Qu Y, Ma T, He Y, et al. Acoustic radiation force optical coherence elastography of corneal tissue.

IEEE J Sel Top Quantum Electron. 2016;22:288–294.
35. Reiser BJ, Ignacio TS, Wang Y, et al. In vitro measurement of rabbit corneal epithelial thickness using ultrahigh resolution optical coherence tomography. *Vet Ophthalmol*. 2005;8:85–88.
36. Moon S, Qu Y, Chen Z. Characterization of spectral-domain OCT with autocorrelation interference response for axial resolution performance. *Opt Express*. 2018;26:7253.
37. Fonck E, Feigl GG, Fasel J, et al. Effect of aging on elastin functionality in human cerebral arteries. *Stroke*. 2009;40:2552–2556.
38. Bizrah M, Yusuf A, Ahmad S. An update on chemical eye burns. *Eye*. 2019;33:1362–1377.
39. Hunter BM, Kallick J, Kissel J, et al. Controlled-potential electromechanical reshaping of cartilage. *Angew Chem Int Ed Engl*. 2016;55:5497–5500.